producing fringes with appreciable contrast was the lack of both temporal and spatial coherence in the X radiation.

At present, Mossbauer sources are the only X-ray sources approaching the desired degree of coherence; however the available intensity is very low. Spatial coherence can be obtained by aperturing (but the aperture must be only a few angstroms) or by moving the subject away from the source. In either case intensity is sacrificed in the pursuit of coherence, and stability problems take over as the limiting factors. Considerations such as these probably mean that X-ray holography is impractical with presently available X-ray sources.

2.4 Beginnings of Optical Holography

First to investigate *optical* holography for its own sake was Rogers [*2.9*]. Working for the most part with a high-pressure mercury arc lamp, Rogers, in 1952, reported a series of experiments which were forerunners of much of the holographic investigation carried out more than a decade later with the laser. Some of the more interesting results were:

1. A hologram made of a hologram (a method now used to copy holograms).
2. Three-dimensional image generation (a possibility recognized by Gabor).
3. Image subtraction by superposition of "negative" and "positive" holograms.
4. Relief, phase holograms (for high diffraction efficiency).
5. An unsuccessful attempt at forming a multicolor-imaging, composite hologram (using color selective dyes).
6. Initiation of work on a computed hologram (a forerunner of recent activity in computer-generated holograms).

Rogers, moreover, pursued Gabor's suggestion that the hologram of a point source is closely related to a Fresnel zone plate. The zone-plate analogy is a useful way of understanding the imaging properties of a hologram and can be derived through simple geometric considerations ([*2.9*], see also El-sum [*2.8*]).

2.4.1 Geometric Analysis of an Elementary Gabor Hologram

As discussed in Section 2.2, Gabor required hologram subjects to be small opaque areas on a relatively large transparent background. In the

analysis to follow, the subject is an idealization of Gabor's subjects, namely a single point scatterer of light. The temporal and spatial coherence properties of the illuminating source are also idealized by assuming a point source of monochromatic spherical waves. Finally, the photosensitive medium recording the hologram is assumed to be thin. With these assumptions the arrangement analogous to Gabor's experiment is shown in Fig. 2.5. A point source S, a distance v from the hologram plane H, illuminates the scattering center P which is a distance u from H. We wish to derive an expression for the intensity of the light pattern on the hologram plane H due to interference of light scattered by P with the background light.

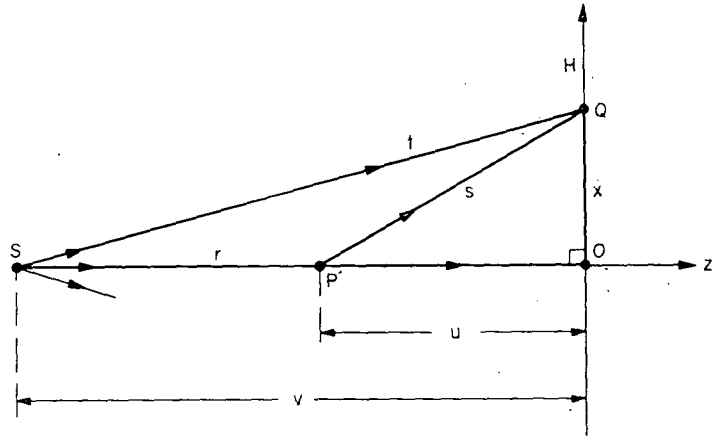

FIG. 2.5. An idealization of Gabor's hologram forming configuration.

The general expression for the intensity of two-beam interference patterns is given by Eq. (1.9),

$$I = I_1 + I_2 + 2a_1a_2 \cos(\varphi_2 - \varphi_1).$$

We assume a hologram is formed whose amplitude transmittance is proportional to I. Diffraction of light illuminating the hologram will result from the spatial variation of the relative phase $\Delta\varphi = \varphi_2 - \varphi_1$ (a_1 and a_2 are nearly constant over the hologram plane). At some point Q on the hologram, $\Delta\varphi$ can be expressed in terms of the difference in path taken by light traveling from S to Q directly (reference wave) compared to that traveling from S to Q via P (subject wave). Assume a continuously oscillating source producing a light wave (of wavelength λ and frequency F) whose absolute phase $\Phi = 2\pi Ft$ is a linear function of the time. A wavefront arriving at

Q at time t_Q has an absolute phase proportional to the time when it was emitted. If the wave velocity is c, then the phase of the wavefront arriving at Q at time t_Q via path SPQ is $\Phi_s = 2\pi F(t_Q - (SPQ/c))$. Similarly, the phase of the wavefront simultaneously arriving at Q via SQ is $\Phi_r = 2\pi F(t_Q - (SQ/c))$. Since $SPQ > SQ$, $\Phi_r > \Phi_s$ and

$$\Phi_r - \Phi_s = \frac{2\pi F}{c}(SPQ - SQ) = \varphi_2 - \varphi_1 = \Delta\varphi = \frac{2\pi\,\Delta l}{\lambda}.$$

Whenever Δl equals $n\lambda$, where $n = 1, 2, 3, \ldots$, $\cos\Delta\varphi = 1$, and the interference fringe has its maximum intensity. The analysis can be confined to the xz plane of Fig. 2.5 since, with S and P each located on the z axis, the intensity pattern is rotationally symmetric about the z axis. From Fig. 2.5

$$\begin{aligned}\Delta l &= (r + s) - t = (v - u + s) - t = v - u + s - t\\ &= v - u + (u^2 + x^2)^{1/2} - (v^2 + x^2)^{1/2}\\ &\approx v - u + u + \frac{x^2}{2u} - v - \frac{x^2}{2v}\\ &= \frac{x^2}{2}\left(\frac{1}{u} - \frac{1}{v}\right),\end{aligned}$$

providing $x \ll u$ and $x \ll v$, as in Gabor's experiment. If we define

$$\frac{1}{f} = \frac{1}{u} - \frac{1}{v}, \tag{2.1}$$

then the condition

$$\Delta l = x_n^2/2f = n\lambda \tag{2.2}$$

determines the radii x_n of the set of maximum brightness, circular fringes centered at O.

2.4.2 The Zone Plate

Solving for x_n in Eq. (2.2), the bright fringes have radii

$$x_n = (f\lambda)^{1/2} \cdot (2n)^{1/2}, \tag{2.3}$$

which are proportional to the square roots of the even integers. The condition, Eq. (2.3), is identical to that defining the transmitting zones of a Fresnel zone plate [*2.10*]. [A zone plate (see Fig. 2.6) can be constructed simply by drawing on white paper concentric circles whose radii are proportional to the square roots of consecutive integers 1, 2, 3,.... These

form annular zones, every other one of which is to be blackened. This done, the figure is photographically reduced to a suitable size, and the resulting transparency is the zone plate [*2.10*].] Since Eq. (2.3) governs the periodicity of the zone plate as well as that of the point source hologram, one would expect their light-diffracting properties to be similar. This is true except that the zones of the zone plate are a square-wave version of the sinusoidal fringes of the hologram grating. A sinusoidal grating diffracts the incident beam only into the $+1$ and -1 orders, the fundamental directions, while the square-wave grating diffracts the beam into higher orders, or harmonics, as well. Thus the diffraction properties of the Gabor hologram can be inferred from the known properties of the zone plate [*2.11*] providing we confine our interest to first-order diffraction.

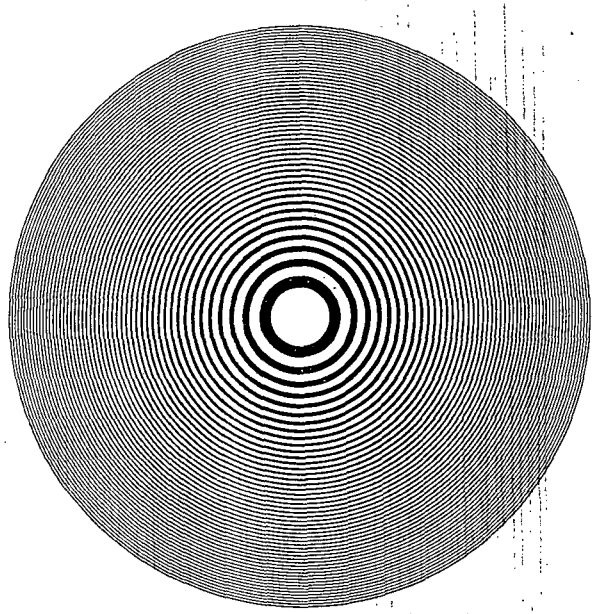

Fig. 2.6. Drawing of a Fresnel zone plate.

The zone plate is a diffraction grating with focusing properties. It is at once both a positive and negative lens. The quantity f in Eq. (2.2) is the focal length of the zone-plate lens and also of the hologram. Equation (2.1) is a *focal equation* defining the lens-to-image distance u in terms of f and the lens-to-subject distance v. As in Fig. 2.7 when a point source S illuminates a zone plate and only first-order diffraction is considered, two images are formed: One is a virtual image P from which the $+1$ order

diffracted waves appear to diverge and the other is a real image P' to which the -1 order diffracted waves converge. By analogy a point-subject hologram also behaves as a diffraction grating with focusing properties and as a negative and positive lens producing virtual and real images. Suppose the hologram is illuminated by the point source S in its original position, a distance v from the hologram. According to Eq. (2.1) the hologram will form a virtual image of S at a distance u from the hologram. The point image can be considered a virtual image of S or better, a virtual image of the original scattering center P, since the image is located at the original site of P. If we choose the latter view, then the spherical wave diffracted from the hologram and appearing to diverge from P can be considered a reconstruction of the wave scattered from P.

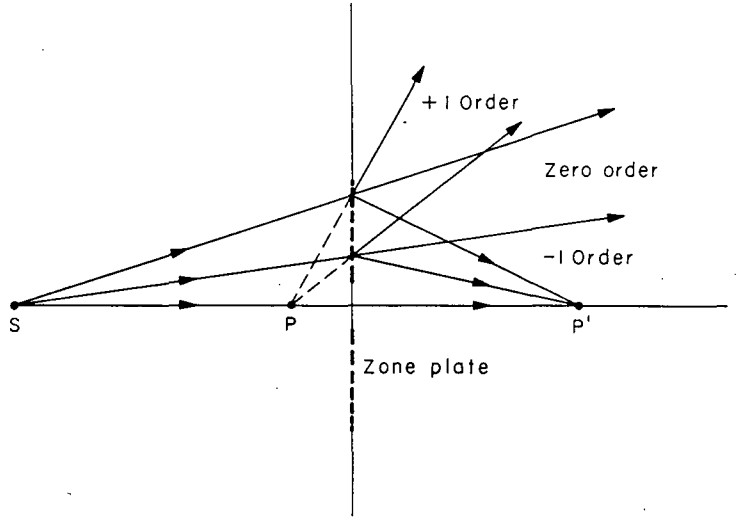

FIG. 2.7. Focusing properties of a zone plate.

The zone-plate behavior of point-subject holograms can be used to explain the imaging properties of more general holograms. A normal, extended subject for a hologram may be thought of as an aggregate of point subjects. Scattered light from each of the points interferes with a reference wave to produce a superposition of many zone-plate-like holograms. (It is assumed that the scattered waves are weak relative to the reference so their mutual interaction can be neglected.) When the entire hologram is illuminated with the reference, each individual hologram generates a virtual image of its associated point subject and, in the process, they combine to image the extended subject.

2.5 In-Line Holograms

Despite a suggestion by Gabor that in the optical regime "where beam splitters are available, methods can be found for providing the coherent background which will allow better separation of object planes and more effective elimination of the twin wave," optical holography in the 1950s continued to be carried out with his original in-line arrangement. Lack of a good source of coherent light probably discouraged experimentation. Source and subject were placed on an optic axis, defined by the normal to the photographic plate. To reveal some of the difficulties and limitations of the method, we return to the analysis initiated by Gabor and used in Section 1.8. There attention is centered on the amplitudes of the arriving and departing waves at the hologram plane.

Suppose we consider an on-axis subject, suitable for a Gabor hologram, to be illuminated with coherent light. The *total* complex amplitude $\mathbf{u}$ of the light striking the photographic plate at the hologram plane can be expressed as a complex function of spatial coordinates where $\mathbf{u} = u_0 \exp(i\varphi_u)$. Part of $\mathbf{u}$ is the undiffracted background or reference wave $\mathbf{r} = r_0 \exp(i\varphi_r)$, and part is the light diffracted by the subject $\mathbf{a} = a_0 \exp(i\varphi_a)$. Thus

$$\mathbf{u} = \mathbf{r} + \mathbf{a}, \tag{2.4}$$

and the intensity I at the hologram plane is

$$\begin{aligned} I &= \mathbf{u}\mathbf{u}^* = (\mathbf{r} + \mathbf{a})(\mathbf{r} + \mathbf{a})^* \\ &= r_0^2 + a_0^2 + \mathbf{r}\mathbf{a}^* + \mathbf{r}^*\mathbf{a} \\ &= r_0^2 + a_0^2 + 2r_0a_0 \cos(\varphi_r - \varphi_a). \end{aligned} \tag{2.5}$$

2.5.1 Response of Photographic Emulsion

Hologram formation on photographic plates requires that photographic emulsion be exposed to the light of intensity I, developed, fixed, and then illuminated by the reference light to produce an image. We inquire as to the response of emulsion to these operations. Hurter and Driffield in 1890 characterized the photographic plate by a curve (called the H&D curve) which is a plot of the *optical density* of the developed plate versus the logarithm of the exposure. They defined the optical density D as

$$D = \log(1/\mathscr{T})$$

where $\mathscr{T}$ is the intensity transmittance, the ratio of the intensity of light

transmitted by the emulsion to that incident on it. The exposure E is defined as

$$E = I_p \tau_e \propto I \tau_e$$

(see Section 1.3) where τ_e is the exposure time and I_p or its abbreviated form I [defined in Eq. (1.1)] is the intensity of the light pattern to which the plate had been exposed. A general form of the H&D curve is shown in Fig. 2.8. Although well suited to photography and used by early holographers, the curve is not the best way to characterize emulsion response for hologram formation (see Section 2.6.2).

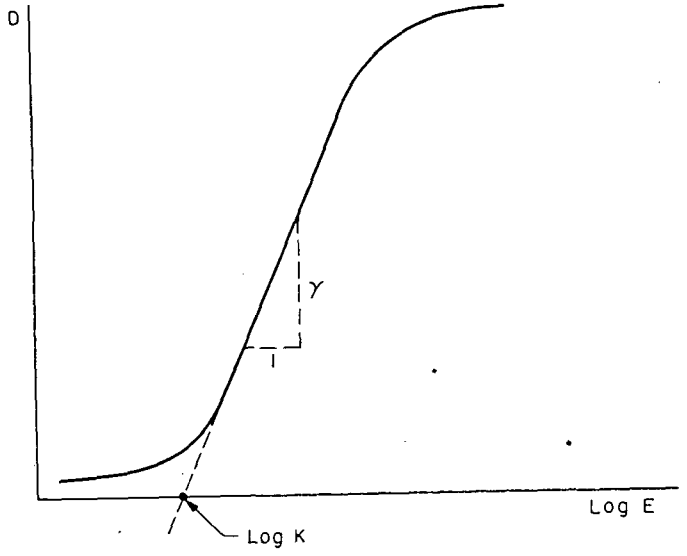

FIG. 2.8. The H&D curve.

The H&D curve is characteristic of both the photographic emulsion and the development procedure. We represent the straight-line portion of the curve by the equations

$$\begin{aligned} D &= \log(1/\mathscr{T}) = \gamma(\log E - \log K), \\ \log(1/\mathscr{T}) &= \log(E/K)^{\gamma}, \end{aligned} \tag{2.6}$$

or

$$\mathscr{T} = K^{\gamma} E^{-\gamma} \propto E^{-\gamma} \propto I^{-\gamma}.$$

In the above, γ is the slope and $\log K$ is the intercept of the linear portion

of the H&D curve extended to the $\log E$ axis. For coherent-light illumination we are generally interested in the *amplitude* transmittance t rather than $\mathscr{T}$, where $t = \sqrt{\mathscr{T}}$, so that

$$t \propto I^{-\gamma/2}. \tag{2.7}$$

Suppose the photographic emulsion, exposed to the intensity I, is developed as a negative. Then the amplitude transmittance is given by

$$t_n \propto I^{-\gamma_n/2}.$$

If, on the other hand, the negative is printed as a positive, the printing illumination producing the positive exposure is proportional to $\mathscr{T}_n$, the intensity transmittance of the negative, and the resulting amplitude transmittance of the print is

$$t_p = (\mathscr{T}_p)^{1/2} \propto (\mathscr{T}_n)^{-\gamma_p/2} \propto (I^{-\gamma_n})^{-\gamma_p/2} \propto I^{\Gamma/2}, \quad \text{where} \quad \gamma_n \gamma_p = \Gamma. \tag{2.8}$$

The subscript "p" refers the previously defined parameters to the positive print.

2.5.2 The Reconstruction

Gabor actually did make a positive hologram. He then illuminated the positive with the original reference wave $\mathbf{r}$. The complex amplitude of the light just after passing through the hologram is

$$\mathbf{w} = \mathbf{r} t_p \propto \mathbf{r} I^{\Gamma/2}.$$

If by proper development Γ is made equal to 2, then

$$\begin{aligned} \mathbf{w} &\propto \mathbf{r}I = \mathbf{r}(r_0^2 + a_0^2 + \mathbf{r}\mathbf{a}^* + \mathbf{r}^*\mathbf{a}) = r_0^2\mathbf{r} + \mathbf{r}a_0^2 + \mathbf{r}\mathbf{r}\mathbf{a}^* + r_0^2\mathbf{a} \\ \mathbf{w} &\propto r_0^2(\mathbf{r} + \mathbf{a}) + r_0^2\big((a_0^2/r_0)\exp(i\varphi_r)\big) + r_0^2\big(\exp(i2\varphi_r)\mathbf{a}^*\big) \end{aligned} \tag{2.9}$$

where $\mathbf{r}\mathbf{r}^* = r_0^2$ and $\mathbf{r} = r_0 \exp(i\varphi_r)$. Providing the reference wave amplitude is uniform over the hologram plate ($r_0^2 =$ constant), the first term on the right of Eq. (2.9) represents a wavefront whose complex amplitude is proportional to that of the original wave $\mathbf{u}$ in Eq. (2.4). If, further, the reference wave is so strong that $a_0^2/r_0 \ll 1$, then the second term can be neglected. Finally for a reference wave whose phase is nearly constant over the hologram plane (as, for example, in the transmission method of forming Gabor holograms), the third term is proportional to the conjugate of the subject wave complex amplitude. It generates a conjugate twin image of the subject.

If the transmission method (Fig. 2.4) is used, the twin image is real (see Section 3.3.1). In this case viewing through the hologram toward the illuminating source, one sees the illuminating source, a virtual image of the subject, and a conjugate real image of the subject. (Recall that an in-line hologram behaves as a set of superimposed zone plates, and the two waves generating the virtual and real images can be reconstructed simultaneously.) If the viewer focuses on the virtual image, its twin, the real image, appears out of focus. On the other hand, if a white screen is placed in the plane where the diffracted rays converge to focus the real image, then out-of-focus light from the virtual image is found to be present. This overlap of light from the twin image in the viewing direction is a handicap of the in-line method which Gabor and his successors strove to eliminate.

2.5.3 Contrast in In-Line Holograms

Before considering some of the methods employed to eliminate the twin image problem, let us inquire as to the effect on the reconstruction of choosing a value for gamma other than $\Gamma = 2$. The complex amplitude of the diffracted waves at the hologram plane can be represented in general form as

$$\begin{aligned}\mathbf{w} \propto \mathbf{r}I^{\Gamma/2} &= \mathbf{r}(r_0^2 + a_0^2 + \mathbf{r}\mathbf{a}^* + \mathbf{r}^*\mathbf{a})^{\Gamma/2} \\ &= \mathbf{r}r_0^{\Gamma}\left(1 + \frac{a_0^2}{r_0^2} + \frac{\mathbf{r}}{r_0^2}\mathbf{a}^* + \frac{\mathbf{r}^*}{r_0^2}\mathbf{a}\right)^{\Gamma/2} \\ &\approx \mathbf{r}r_0^{\Gamma}\left(1 + \frac{\Gamma}{2}\frac{a_0^2}{r_0^2} + \frac{\Gamma}{2}\frac{\mathbf{r}}{r_0^2}\mathbf{a}^* + \frac{\Gamma}{2}\frac{\mathbf{r}^*}{r_0^2}\mathbf{a} + \cdots\right).\end{aligned}$$

Assuming $r_0^2 \gg a_0^2$ so that the second term is negligible and multiplying through by the factor $\mathbf{r}$, we have

$$\mathbf{w} \propto r_0^{\Gamma}\left(\mathbf{r} + \frac{\Gamma}{2}\mathbf{a}\right) + \text{the conjugate real-image term.}$$

Focusing on the virtual image and neglecting the unfocused real-image light,

$$\mathbf{w} \propto \mathbf{r} + \frac{\Gamma}{2}\mathbf{a}. \tag{2.10}$$

Equation (2.10) tells us that the value of gamma controls the contrast, i.e., it controls the ratio of the signal amplitude to the background. For example, when $\Gamma = +2$ (positive hologram) then $\mathbf{w}$ is a reconstruction of the original wave $\mathbf{u} = \mathbf{r} + \mathbf{a}$ where the subject light adds to the background; when $\Gamma = -2$ (negative hologram) then $\mathbf{w} = \mathbf{r} - \mathbf{a}$ and the subject light is subtracted from the background. In the latter case the result is a negative image. Values of Γ between $+2$ and -2 produce varying degrees of contrast.

2.5.4 Elimination of the Twin Image Problem

We have seen that in-line holograms, as formed by early holographers, require: (1) subjects consisting of small opaque objects on a large transparent background so that $r_0^2 \gg a_0^2$, (2) a positive print to be made of the original exposure, and (3) the overall gamma to be $+2$ to maintain original contrast in the subject. While these requirements were restrictive, it was the overlap of one unfocused image onto its twin focused image that seemed most hampering. Several early attempts were made to eliminate the unwanted image light while still maintaining the in-line geometry. The first of such attempts was the two-hologram method of Bragg and Rogers [*2.12*]. Their procedure is straightforward: A subject, suitable for an in-line hologram, is illuminated with parallel coherent light and its diffraction pattern recorded in Hologram 1. If, after development, the hologram is replaced and the subject removed, illumination by the original source generates a virtual image of the subject at the original subject position $u = -f$ [see Eq. (2.1) for $v = \infty$]. A real image is also formed at a distance f on the far side of the hologram. However, in the plane of the real image is also the unwanted diffraction pattern produced by the wave appearing to diverge from the virtual image. Since the virtual image and the subject occupied identical positions, $2f$ units distant from the real image plane, it was clear to Bragg and Rogers that the unwanted diffraction pattern was identically that of the subject observed at a distance of $2f$. They suggested that a *negative* photographic record of the subject diffraction pattern be made at a distance $2f$ from the subject. This, then, is the second hologram.

To observe the real image and simultaneously eliminate disturbance from its twin, one must illuminate Hologram 1 in its original position and register Hologram 2 with the disturbing pattern in the real image plane. The negative record on Hologram 2 should just cancel the actual pattern received from the virtual image; remaining should be the real image on a uniform background. In practice the cancellation is imperfect, and the method at best only partially successful. Moreover it introduces noise and applies only to the real image.

El-Sum [*2.7*] suggested other methods for eliminating the twin image, and Lohmann [*2.13*] proposed a method involving filtering the Fraunhofer diffraction pattern. Neither these nor the Bragg–Rogers method proved

entirely effective nor were they very convenient or flexible. The problem remained one of major importance. Before considering Leith's and Upatnieks' solution to the twin image problem, we note that, in certain cases, the in-line hologram is capable of producing the desired image without undue interference from the twin image. Using the in-line method, Thompson *et al.* [*2.14*] were able to form pulsed-laser holograms of moving aerosol particles. (The available pulsed lasers lacked sufficient coherence length, so the in-line method seemed a good choice.) Aerosol particles are so small that a hologram made in the near field of the ensemble of particles is still in the far field of any individual particle. If one examines the real image of a particle, its virtual image appears to lie in a plane a long distance away. Hence, at the real image plane, the diffraction pattern of the point-like virtual image appears as an unobtrusive uniform background, a spherical wave of constant amplitude. The real image may therefore be clearly observed.

2.6 Off-Axis Holograms

By breaking with the in-line geometry concept and introducing the reference beam at an angle to the subject beam, Leith and Upatnieks devised the most general and successful method of separating the twin image (as well as undiffracted light) from the desired image. Figure 2.9 indicates the arrangement initially employed by Leith and Upatnieks [*2.15*] with a mercury discharge light source. Two lines from the Fraunhofer diffraction pattern of a line grating are selected as phase-related secondary sources.

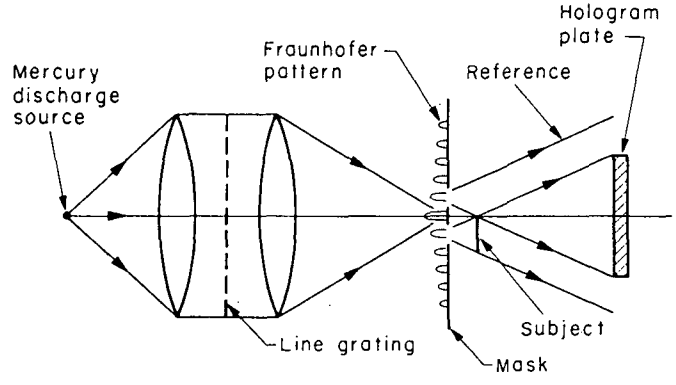

FIG. 2.9. Initial arrangement used by Leith and Upatnieks to form an off-axis hologram. [After E. Leith and J. Upatnieks, *J. Opt. Soc. Amer.* **52**, 1123 (1962).]

One of these acts as the reference wave source while the other transilluminates a subject. The hologram can be formed anywhere in the region of beam overlap. The resemblance of the experimental arrangement to that of Young is apparent.

While it is perhaps more appropriate to delay the explanation of the off-axis method till after the spatial frequency domain concept has been introduced (Chapter 5), some of the obvious benefits can be appreciated by returning to a zone-plate picture. Consider Fig. 2.10 which indicates a zone-plate pattern formed by interference of a plane wave reference with the spherical wave scattered by a point scatterer at *P*. The in-line procedure entails placing a small photographic plate (the dashed-line rectangle) at the center of the pattern such that its normal passes through *P* and is parallel to the direction of propagation of the reference plane wave. When nonlaser sources are used, the portion of the interference pattern which can be recorded as a hologram is generally confined to a small radius about the center, because of the limited coherence length of the light. As the light

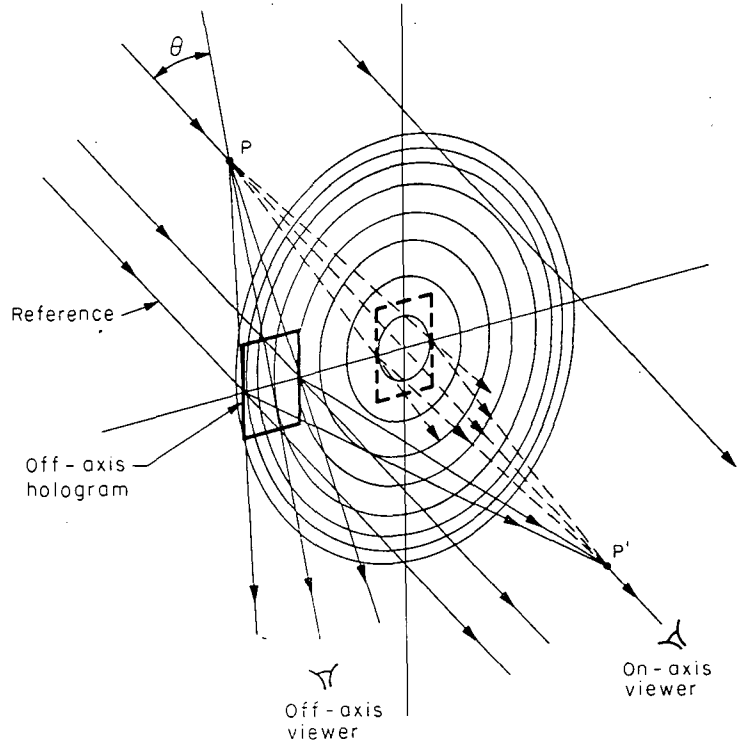

FIG. 2.10. A simple hologram recorded off axis.

path from source to hologram plane via the subject increases over the direct path via the reference wave and the difference approaches the coherence length of the source, the interference fringe visibility becomes zero and the record of the interference no longer diffracts with useful efficiency. One can see from Fig. 2.10 that the path difference increases as one proceeds out from the center of the interference pattern. The small hologram that can be formed is illuminated by the plane wave reference and diffracts a wave appearing to diverge from a virtual image at P and a second wave converging to a real image at P'. On-axis observation of either image is disturbed by the out-of-focus light from the other and by the undiffracted illumination as well.

Suppose, however, that the coherence length of the light is sufficient to produce useful fringe visibility over a large portion of the zone-plate pattern such that the small photographic plate can be moved so far off axis that it intercepts no axial rays from P. Then, as indicated in the figure, the rays diverging from the virtual image at P are all angularly separated from those converging to P', and the twin image problem is eliminated. That portion of the illuminating reference wave emerging undiffracted from the hologram is also angularly separated from the image waves. [Referring to Eq. (2.5), we note that the subject wave intensity a_0^2 is recorded on the hologram along with the interference terms and the constant reference intensity. The illuminating reference wave also diffracts from any spatial modulation of the hologram optical density due to a_0^2. Thus θ, in Fig. 2.10, must be taken large enough to avoid overlapping the image waves with transmitted illumination diffracted by a_0^2. For general subjects the interaction with a_0^2 results in diffracted light confined to some angular range centered on the reference direction.]

2.6.1 Contrast in Off-Axis Holograms

Since the diffracted image wave and the transmitted illuminating wave do not overlap in viewing space, the reconstruction presented to the observer of, say, the virtual-image wavefront is represented by only the second term in Eq. (2.10), $\frac{1}{2}\Gamma\mathbf{a}$. The value or sign of Γ no longer governs the contrast in this case. If Γ were chosen to be -2, the generated image would no longer be a negative of the original. The observed image-wave intensity, given by $(-\frac{1}{2}\Gamma\mathbf{a})(-\frac{1}{2}\Gamma\mathbf{a}^*)$, is still proportional to the original wave intensity and will yield a positive image. Thus only a single negative hologram is necessary to produce a positive image whose contrast is that of the original subject.

2.6.2 Linear Response

With the advent of the off-axis method it became clear that characterization of photographic emulsion by the slope of the linear region of its H&D curve is inconvenient [*2.16*]. Of course any method of characterization must be directed toward achieving a recording which faithfully reconstructs the subject wave when illuminated by the reference wave. Fidelity is obtained when the *amplitude transmittance* of the developed hologram is linearly proportional to the intensity of the interference pattern. Then the virtual image wave, as given in Eq. (2.9), is $r_0^2\mathbf{a}$ and proportional to $\mathbf{a}$, providing r_0^2 is constant over the hologram. Therefore an exposure characteristic of significance to holography is the plot of the amplitude transmittance t versus exposure E as shown in Fig. 2.11a. A proper exposure for holography

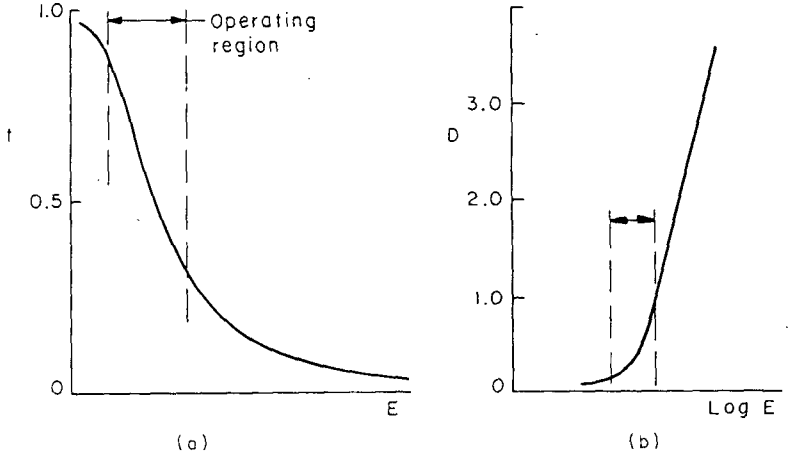

FIG. 2.11. (a) Amplitude transmittance versus exposure. (b) The H&D curve showing the location of the linear region of the curve in (a). [After H. Kogelnik, "Reconstructing Response and Efficiency of Hologram Gratings," *Proc. Symp. Mod. Opt.*, New York, 1967, p. 605. Polytechnic Press, Brooklyn, New York, 1967.]

will produce an amplitude transmittance having values within the limits of the linear portion of the curve. If the maxima or minima of the intensity pattern, to which the hologram plate is exposed, produce transmittance values corresponding to the nonlinear portion of the curve, distortions will be observed in the reconstruction. Figure 2.11b shows that the linear region of the t versus E plot for the commonly used Eastman Kodak 649F emulsion lies at the toe of the H&D curve. In this case the latter provides little guidance in selecting the exposure limits. It is interesting to note that the average

exposure value, corresponding to the center of the linear region of the t versus E curve, is considerably less than that corresponding to the center of the linear region of the H&D curve. Hence, for a given emulsion, hologram exposures are generally shorter than those for normal photographs and the plates are less dense (see Fig. 1.1).

2.6.3 Further Effects of the Off-Set Reference and Increased Coherence

Introduction of the off-axis technique had the effect of freeing optical holography from restraints originating in the early work with electron waves and X rays. It became evident that by using beam splitters one no longer needed to derive the reference from undiffracted light passing through the subject, even in the in-line case. This together with the increased coherence of laser light allowed holography to be applied to the general class of transmitting or reflecting objects, e.g., continuous tone transparencies and reflecting three-dimensional solids.

The in-line hologram requirement that the reference intensity greatly exceed the subject wave intensity need not be met with the reference beam off set. However, the reference intensity must be large enough compared to its modulation (by the subject wave) to prevent the resultant exposure from swinging beyond the bounds of the linear portion of the t versus E curve.

REFERENCES

2.1. W. L. Bragg, "An Optical Method of Representing the Results of X-Ray Analyses," *Z. Kristallogr. Kristallgeometrie Kristallphys. Kristallchem.* **70**, 475 (1929).

2.2. W. L. Bragg, "A New Type of 'X-Ray Microscope,' " *Nature* **143**, 678 (1939).

2.3. W. L. Bragg, "The X-Ray Microscope," *Nature* **149**, 470 (1942).

2.4. D. Gabor, "A New Microscopic Principle," *Nature* **161**, 777 (1948).

2.5. M. E. Haine and J. Dyson, "A Modification to Gabor's Proposed Diffraction Microscope," *Nature* **166**, 315 (1950).

2.6. M. E. Haine and T. Mulvey, "The Formation of the Diffraction Image with Electrons in the Gabor Diffraction Microscope," *J. Opt. Soc. Amer.* **42**, 763 (1952).

2.7. H. M. A. El-Sum and P. Kirkpatrick, "Microscopy by Reconstructed Wave-Fronts," *Phys. Rev.* **85**, 763 (1952).

2.8. H. M. A. El-Sum, "Reconstructed Wavefront Microscopy," Ph. D. Thesis, Stanford Univ. (1952). (Available from Univ. Microfilm Inc., Ann Arbor, Michigan.)

2.9. G. L. Rogers, "Experiments in Diffraction Microscopy," *Proc. Roy. Soc. (Edinburgh)* **63A**, 193 (1952).

2.10. O. E. Myers, Jr., "Studies of Transmission Zone Plates," *Amer. J. Phys.* **19**, 359 (1951).

2.11. M. Sussman, "Elementary Diffraction Theory of Zone Plates," *Amer. J. Phys.* **28**, 394 (1960).

2.12. W. L. Bragg and G. L. Rogers, "Elimination of the Unwanted Image in Diffraction Microscopy," *Nature* **167**, 190 (1951).

2.13. A. Lohmann, "Optische Einseitenbandübertragung angewandt auf das Gabor-Mikroskop." *Opt. Acta* **3**, 97 (1956).

2.14. B. J. Thompson, J. Ward, and W. Zinky, "Application of Hologram Techniques for Particle-Size Determination," *J. Opt. Soc. Amer.* **55**, 1566A (1965); *Appl. Opt.* **6**, 519 (1967).

2.15. E. N. Leith and J. Upatnieks, "Reconstructed Wavefronts and Communication Theory," *J. Opt. Soc. Amer.* **52**, 1123 (1962).

2.16. A. Kozma, "Photographic Recording of Spatially Modulated Coherent Light," *J. Opt. Soc. Amer.* **56**, 428 (1966).

Chapter 3

GEOMETRIC ANALYSIS OF POINT-SOURCE HOLOGRAMS

In Chapter 2 the Gabor in-line hologram and the Leith–Upatnieks off-axis hologram were described in terms of the interference of light coming from two point sources. Despite the simplifications involved, such point-source holograms clearly illustrate many of the basic features of holography. From them much can be learned about the spacing of the interference fringes to be recorded, about properties of the virtual and real images that are generated, and about the magnification obtainable in the reconstruction process.

There are no point sources of light in the physical world, but the extended sources and illuminated subjects we do encounter can be thought of as collections of point sources. Let us suppose that $\mathbf{a}_1$, $\mathbf{a}_2$, ..., etc. represent the complex amplitudes of light waves arriving at the hologram plane from one such collection of subject point sources. If $\mathbf{r}$ represents the reference light complex amplitude arriving at the hologram, then the total complex amplitude at the hologram is

$$\mathbf{a}_1 + \mathbf{a}_2 + \cdots + \mathbf{r}.$$

The quantity important to the holographic recording process is the total intensity

$$\begin{aligned} I &= (\mathbf{a}_1 + \mathbf{a}_2 + \cdots + \mathbf{r})(\mathbf{a}_1^* + \mathbf{a}_2^* + \cdots + \mathbf{r}^*) \\ &= \mathbf{a}_1\mathbf{a}_1^* + \mathbf{a}_2\mathbf{a}_2^* + \cdots + \mathbf{r}\mathbf{r}^* + (\mathbf{a}_1\mathbf{a}_2^* + \mathbf{a}_2\mathbf{a}_1^* + \cdots) \\ &\quad + \mathbf{r}(\mathbf{a}_1^* + \mathbf{a}_2^* + \cdots) + \mathbf{r}^*(\mathbf{a}_1 + \mathbf{a}_2 + \cdots). \end{aligned}$$

Apart from the intermodulation terms (the terms $\mathbf{a}_1\mathbf{a}_2^* + \mathbf{a}_2\mathbf{a}_1^* + \cdots$), which indicate interference among the subject wave components, the subject point sources behave independently. Concern with effects of the intermodulation terms on reconstruction can be removed in the ways touched on in Chapter 2. For the case of in-line holography, the reference wave amplitude is made much larger than the subject wave amplitude. The intermodulation terms then become negligible. In the case of off-axis holography, the angle between subject and reference waves is chosen large enough to angularly separate the image waves from the waves diffracted by the intermodulation terms. (The latter waves propagate in directions close to that of the illuminating beam.)

Since the subject point sources can for our purposes be regarded as independent, we restrict our attention here to a *single* subject point source and to the holograms formed with a reference point source. We assume all waves travel from left to right. We further assume that (1) all illumination is perfectly coherent, (2) the holograms are exposed and developed to produce an amplitude transmittance proportional to the intensity of the interference pattern, and (3) the holograms behave as plane diffraction gratings.

The reader who anticipates making his own holograms and seeks to observe the results and properties described in this chapter should be forewarned regarding the choice of recording media. Many of the effects to be discussed, e.g., simultaneous observation of real and virtual images and the results of illuminating the hologram at a different angle or with a different wavelength than that used to form it, can best be observed when the hologram truly behaves as a plane diffraction grating. The high-resolution photographic emulsions normally used in holography range from 6 to 15 μm in thickness; therefore small reference-to-subject beam angles must be employed to avoid the angular and spectral selective properties of volume-grating behavior. One recording material thin enough to behave essentially as a plane diffraction grating is thermoplastic ([*3.1*], see also Chapter 10). Holograms formed in it will exhibit the properties we shall analyze.

3.1 Computation of Subject–Reference Phase Differences

In the analysis to follow, a subject, reference, or illuminating wave arriving at any point Q on the hologram plane in Fig. 3.1 is to be represented by the difference in its phase at Q over its phase at a fixed point of origin O. (It is assumed that the amplitude of the spherical wave arising

from each point source is approximately uniform across the hologram plane and therefore plays no part in the essential process.) If we assume that the space on either side of the hologram has the same index of refraction and if the hologram can be regarded as very thin, then relative phase can be computed from geometrical light-path differences. We shall employ the basic analysis introduced by Meier [*3.2*]. It involves making paraxial approximations. (For a nonparaxial analysis see Champagne [*3.3*].)

Let $\mathbf{a} = a_0 \exp(i\varphi_a)$ be the complex amplitude of the light arriving at the hologram plane from the subject point source and let $\mathbf{r} = r_0 \exp(i\varphi_r)$ be the complex amplitude of the reference wave at the hologram. Then, as in Section 2.5 (but without restriction to the in-line configuration), the intensity recorded at the hologram plane is

$$I = a_0^2 + r_0^2 + \mathbf{ra}^* + \mathbf{r}^*\mathbf{a}. \tag{3.1}$$

We are primarily interested in the interference terms

$$\mathbf{ra}^* + \mathbf{r}^*\mathbf{a} = 2a_0 r_0 \cos(\varphi_r - \varphi_a) \tag{3.2}$$

which describe the periodic spatial variation of intensity in the interference fringes. The periodicity of the hologram fringes is governed by the argument of the cosine, i.e., by the phase difference $\varphi_r - \varphi_a$.

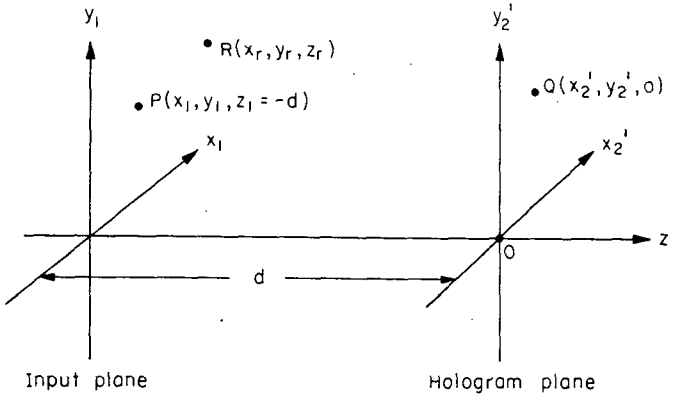

FIG. 3.1 Parameters required for computation of $\varphi_r - \varphi_a$.

Consider now hologram formation as indicated in Fig. 3.1. The subject point source P is in the x_1y_1 plane, $z_1 = -d$ units from the origin O of the z axis. The origin O is located in the hologram $x_2'y_2'$ plane. (The primes will be carried until we reach that stage of the analysis where enlargement

of the hologram plane is considered.) A reference point source R is located in some arbitrary plane $x_r y_r$, a distance z_r from the hologram plane. If R is to the left of the hologram plane and the reference wave diverges from R, z_r is negative (as shown); if R is to the right of the hologram plane and the reference wave converges to R, z_r is positive. We wish to compute $\varphi_r - \varphi_a$ at an arbitrary point Q in the hologram plane. We can differentiate $(1/2\pi)(\varphi_r - \varphi_a)$ with respect to a spatial coordinate to determine the number of cycles of intensity variation per unit distance along the coordinate axis. We then know how many fringes per unit distance in that direction must be recorded by the photographic emulsion as a function of the arrangement of P, R, and the recording plate.

The starting phases of the waves emanating from P and R are perfectly arbitrary. Let us assume that these have been adjusted so that each wave has the same phase at the point O in the hologram plane. We can call that phase value zero. Since P and R are point sources, they each emit a spherical wave whose phase at any point in space is proportional to the radial distance of that point from the source. Then, by computing the path difference $PQ - PO$, we obtain the phase φ_a of the light complex amplitude at Q coming from P. By similar computation we obtain the phase φ_r of the light complex amplitude at Q coming from R. The sign of the phase at Q relative to that at O must be carefully considered. The two diagrams of Fig. 3.2

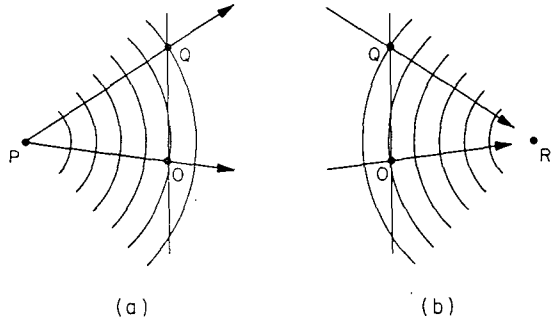

FIG. 3.2. Aid in determination of the signs of relative phase at Q and O for (a) a diverging subject wave and (b) a converging reference wave.

are useful in discussing this point. The magnitude of the phase difference φ_a, corresponding to the path difference $PQ-PO$, is $|\varphi_a| = (2\pi/\lambda)|(PQ-PO)|$ where λ represents the wavelength. If P is a real point source of diverging spherical waves and if $PQ > PO$, then the wavefront arriving at Q was emitted at an earlier time than that simultaneously arriving at O (see Fig.

3.2a). Therefore its phase at Q must be less than that of the front at O (assuming phase to increase with time), and consequently $\varphi_a = -(2\pi/\lambda) \times (PQ - PO)$. In Fig. 3.2b a converging reference wave is indicated. Here R exists as an effective point focus on the opposite side of the hologram from P. For $RQ > RO$, the phase of the wavefront at Q is greater than at O since the wavefront at Q was emitted later. Thus, for a *converging* reference wave, $\varphi_r = +(2\pi/\lambda)(RQ - RO)$, while for the usual case of a *diverging* reference wave, $\varphi_r = -(2\pi/\lambda)(RQ - RO)$.

We can now return to the computation of $\varphi_r - \varphi_a$ for the case where P and R are each sources of diverging light on the same side of the hologram. For the phase of the subject wave at Q, $\varphi_a(x_2', y_2')$,

$$\varphi_a = -\frac{2\pi}{\lambda_1}(PQ - PO)$$

$$= -\frac{2\pi}{\lambda_1}\{[(x_2' - x_1)^2 + (y_2' - y_1)^2 + z_1^2]^{1/2} - [x_1^2 + y_1^2 + z_1^2]^{1/2}\}$$

$$= +\frac{2\pi}{\lambda_1} z_1 \left\{\left[1 + \frac{(x_2' - x_1)^2 + (y_2' - y_1)^2}{z_1^2}\right]^{1/2} - \left[1 + \frac{x_1^2 + y_1^2}{z_1^2}\right]^{1/2}\right\},$$

where λ_1 is the wavelength of the light used to form the interference pattern and where we understand z_1 to have a *negative* value so that the sign of φ_a remains negative. (Thus the character of the wave, i.e., diverging or converging, is carried implicitly in z_1.) If both P and Q are not far off the z axis, and if z_1 is large enough, φ_a can be approximated to the first order in $1/z_1$ by

$$\varphi_a \approx \frac{2\pi}{\lambda_1}\left[\frac{1}{2z_1}(x_2'^2 + y_2'^2 - 2x_2'x_1 - 2y_2'y_1)\right]. \tag{3.3}$$

The next higher-order terms in the binomial expansion are third-order in $1/z_1$. [The first-order approximation will be satisfactory for most of the purposes of this chapter. We shall point out when an expression derived in this chapter with the aid of Eq. (3.3) differs, because of the approximation, from that obtained through other considerations.] $\varphi_r(x_2', y_2')$, the reference phase at Q, obtained in a fashion analogous to that used for φ_a, is

$$\varphi_r \approx \frac{2\pi}{\lambda_1}\left[\frac{1}{2z_r}(x_2'^2 + y_2'^2 - 2x_2'x_r - 2y_2'y_r)\right]. \tag{3.4}$$

The subject–reference phase difference at Q is then given by

$$\varphi_r - \varphi_a = \frac{2\pi}{\lambda_1}\left[(x_2'^2 + y_2'^2)\left(\frac{1}{2z_r} - \frac{1}{2z_1}\right) - x_2'\left(\frac{x_r}{z_r} - \frac{x_1}{z_1}\right) - y_2'\left(\frac{y_r}{z_r} - \frac{y_1}{z_1}\right)\right]$$

$$= \frac{2\pi}{\lambda_1}\Delta l. \tag{3.5}$$

The quantity in the brackets is the path difference Δl for light traveling to Q from P as against that traveling to Q from R.

3.1.1 The In-Line Hologram

Both subject and reference point sources are on-axis in the case of the in-line hologram so that in Eq. (3.5), x_1, y_1, x_r, and y_r are all zero. If we relabel $z_1 = -u$ and $z_r = -v$ to correspond with the notation of Section 2.4.1, then the path difference in Eq. (3.5) becomes

$$\Delta l = (x_2'^2 + y_2'^2)\left(\frac{1}{2}\right)\left(\frac{1}{z_r} - \frac{1}{z_1}\right)$$

$$= (x_2'^2 + y_2'^2)\left(\frac{1}{2}\right)\left(\frac{1}{u} - \frac{1}{v}\right) = \frac{(x_2'^2 + y_2'^2)}{2f} = \frac{\varrho^2}{2f} \tag{3.6}$$

where we have used Eq. (2.1), $f^{-1} = u^{-1} - v^{-1}$, and where ϱ is the radial distance from the origin O at the hologram plane. The bright fringes of the interference pattern occur whenever $\Delta l = n\lambda_1$ where n is an integer. Since Δl is symmetric about the origin, the fringes are circular and form the zone plate pattern given by

$$\Delta l = \frac{x_2'^2 + y_2'^2}{2}\left(\frac{1}{u} - \frac{1}{v}\right) = \frac{\varrho^2}{2f} = n\lambda_1. \tag{3.7}$$

As stated in Eq. (3.2) the spatial variation of the interference pattern intensity is governed by a cosine function, $\cos(\varphi_r - \varphi_a) = \cos(2\pi\,\Delta l/\lambda_1)$. If Δl were linearly dependent on the spatial variable, then a constant frequency could be ascribed to the cosinusoidal intensity variation. This is generally not the case, but a *local* spatial frequency, the fringe frequency $\nu(\varrho)$, can be defined. (Here ϱ is the spatial variable measured along a direction perpendicular to the crests of the interference pattern, and ν is considered to be a function of ϱ.) We define ν as the spatial rate of change of

the phase of the intensity pattern at Q divided by 2π radians:

$$\nu(\varrho) = \frac{\partial(\varphi_r - \varphi_a)}{\partial\varrho} \cdot \frac{1}{2\pi} = \frac{\partial}{\partial\varrho}\left(\frac{\Delta l}{\lambda_1}\right). \tag{3.8}$$

For Δl given in Eq. (3.7),

$$\nu(\varrho) = \varrho/f\lambda_1. \tag{3.9}$$

Thus, proceeding radially outward from the hologram center, the fringe frequency increases linearly with ϱ. At some value of ϱ, ν may exceed the resolution capability ν_m of the photosensitive medium. Such a radius defines the limiting aperture and the image resolution of the hologram.

When comparing the recording resolution requirements of in-line holograms with other hologram-forming configurations to be analyzed in this chapter, we shall find it convenient and sufficient to consider only ξ' the fringe frequency component of ν along the x_2' direction. As a further simplification we consider R to be at infinity (a plane wave reference with $z_r = \infty$). For this case [see Eq. (3.6)]

$$\xi' = \frac{\partial(\varphi_r - \varphi_a)}{2\pi\,\partial x_2'} = -\frac{x_2'}{z_1\lambda_1}. \tag{3.10}$$

The farther the subject is from the hologram, the coarser and the more easily recorded are the fringes. Gabor attempted to apply this fact in his "projection method" (Section 2.2). Unfortunately image resolution decreases as well if x_2' is limited.

3.1.2 The Off-Axis Hologram

The relation obtained by setting $\Delta l = n\lambda_1$ in Eq. (3.5),

$$\Delta l = (x_2'^2 + y_2'^2)\left(\frac{1}{2}\right)\left(\frac{1}{z_r} - \frac{1}{z_1}\right) - x_2'\left(\frac{x_r}{z_r} - \frac{x_1}{z_1}\right) - y_2'\left(\frac{y_r}{z_r} - \frac{y_1}{z_1}\right) = n\lambda_1, \tag{3.11}$$

is the general expression for a circle whose center has the coordinates

$$x_2' = \frac{z_1x_r - z_rx_1}{z_1 - z_r}, \qquad y_2' = \frac{z_1y_r - z_ry_1}{z_1 - z_r}, \tag{3.12}$$

and whose radius ϱ is given by

$$\varrho^2 = \left(\frac{z_1x_r - z_rx_1}{z_1 - z_r}\right)^2 + \left(\frac{z_1y_r - z_ry_1}{z_1 - z_r}\right)^2 + \frac{2n\lambda_1z_1z_r}{z_1 - z_r}. \tag{3.13}$$

Suppose we consider the off-axis intensity pattern formed by the interference of an axial plane wave reference ($x_r = y_r = 0$, $z_r = \infty$) with a spherical subject wave diverging from an off-axis point (x_1, $y_1 = 0$, z_1). The center of the set of circular fringes, whose radii correspond to integral values of n in Eq. (3.13), is given by Eq. (3.12) as $x_2' = x_1$ and $y_2' = 0$. A zone-plate pattern is thus centered at the foot of the perpendicular dropped from P to the hologram plane. The situation is indicated in Fig. 3.3. If the

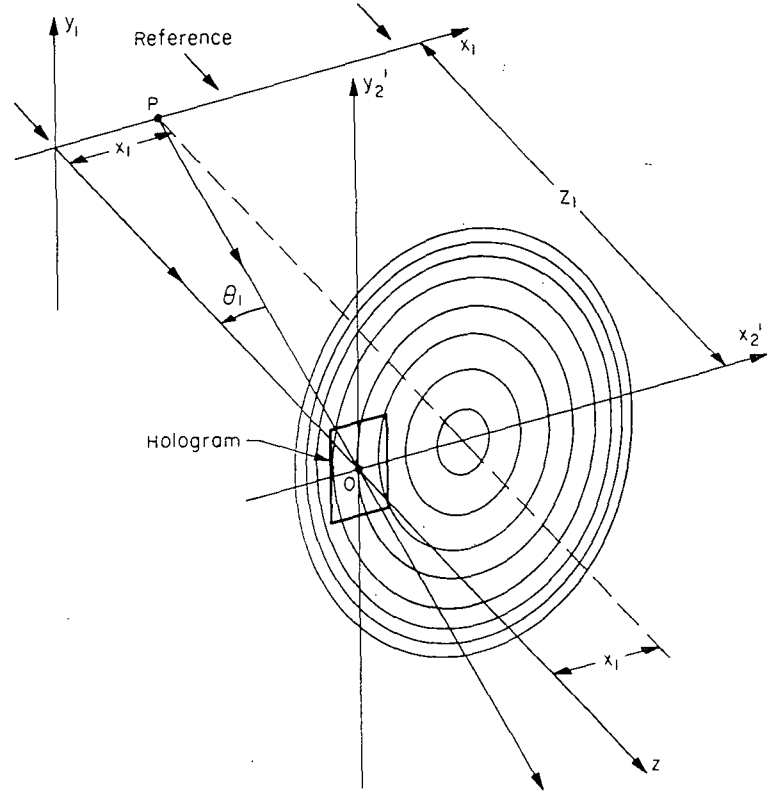

FIG. 3.3. Hologram produced by off-axis subject P and axial plane wave reference.

photographic plate is centered at O so that it can record only off-center portions of the interference pattern, a Leith–Upatnieks hologram is obtained. The fringe frequency ξ' in the x_2' direction can be found by differentiating $\Delta l/\lambda_1$ in Eq. (3.11) under the conditions $x_r = y_r = y_1 = 0$ and $z_r = \infty$. The result is

$$\xi' = -\frac{x_2'}{z_1\lambda_1} + \frac{x_1}{z_1\lambda_1}. \tag{3.14}$$

Assuming the hologram plate to be centered at O, let us compare ξ' in Eq. (3.14) with that found for the in-line configuration, Eq. (3.10). At the hologram center ($x_2' = 0$) the in-line fringe frequency is zero while the off-axis fringe frequency is $x_1/z_1\lambda_1$. As one proceeds outward in the negative x_2' direction (see Fig. 3.3), the frequency of each fringe system increases linearly with x_2' and this frequency difference is maintained. At the edge of the hologram are generated the highest frequencies to be recorded. If the photosensitive medium on the hologram plate is to record the fringes in the off-axis case, it must have a resolution capability $x_1/z_1\lambda_1$ in addition to that required for the in-line case. Examination of Eq. (3.11) reveals that had we considered an off-axis reference plane wave ($x_r \neq 0$, $x_r/z_r = \tan\theta_r \approx \theta_r$), the frequency difference would in that case be

$$\left(\frac{x_1}{z_1} - \frac{x_r}{z_r}\right)\frac{1}{\lambda_1} \approx \frac{\theta_1 - \theta_r}{\lambda_1} \tag{3.15}$$

where θ_1 is the mean angle to the axis made by the subject wave, i.e., the angle to the z axis made by a ray passing from P to the center of the hologram at O. Thus the mean angle between subject and reference beam provides the difference in the maximum fringe frequency generated in an off-axis hologram as against the in-line hologram.

In the practical case of an extended subject, either the width of the subject or the width of the recording plate can cause the fringe frequency ξ' to exceed the plate resolution ν_m. When the plate is small compared to the subject, the last term in Eq. (3.14) [or $(\theta_1 - \theta_r)/\lambda_1$ in Eq. (3.15)] is dominant. Point sources at the extreme dimension of the subject produce the maximum fringe frequency at the plate. If $\xi' > \nu_m$ for the extreme portions of the subject, then such portions are not recorded. On the other hand, when the plate is much larger than the subject, the dominant term in Eq. (3.14) might be the first. Beyond some value of x_2' all subject points produce zone-plate fringes whose frequency $\xi' > \nu_m$. That value of x_2' defines the practical extent of the hologram record.

3.1.3 Lensless Fourier Transform Hologram

We consider now the arrangement shown in Fig. 3.4 where subject and reference points are in the same plane. The coordinates of the subject point P are (x_1, $y_1 = 0$, z_1) and those of the reference point R are (x_r, $y_r = 0$, $z_r = z_1$). The phase difference $\varphi_r - \varphi_a$ in Eq. (3.5) becomes

$$\varphi_r - \varphi_a = -\frac{2\pi}{\lambda_1}\left(\frac{x_r}{z_1} - \frac{x_1}{z_1}\right)x_2'. \tag{3.16}$$

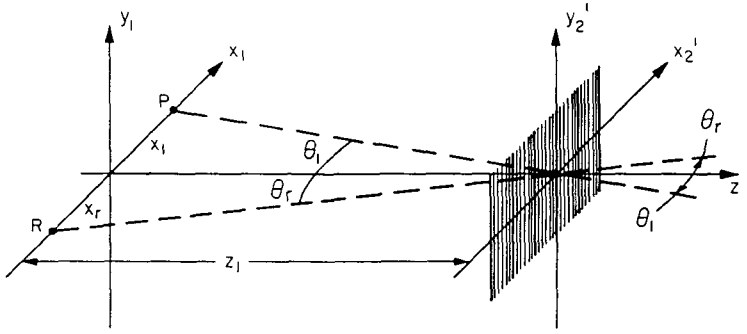

FIG. 3.4. Lensless Fourier-transform hologram configuration. (*Note*: θ_1 is a negative angle while θ_r is positive.)

Differentiation of $(\varphi_r - \varphi_a)/2\pi$ with respect to x_2' yields the *constant* fringe frequency

$$\xi' = \frac{x_1 - x_r}{z_1\lambda_1}. \tag{3.17}$$

Since the intensity of the interference pattern is independent of y_2', as is apparent from Eq. (3.16), the fringes are vertical, uniformly spaced, *linear* fringes. Their intensity varies cosinusoidally in the x_2' direction. (The physical arrangement and results are equivalent to those of Thomas Young's experiment. The method was suggested by Winthrop and Worthington for X-ray holography [*3.4*] and by Stroke for optical holography [*3.5*].)

As may be seen in Fig. 3.4, the ratio $x_r/z_1 = \tan\theta_r \approx \theta_r$ in our first-order approximation, and similarly the ratio $x_1/z_1 \approx \theta_1$. We can write $\varphi_r - \varphi_a$ in Eq. (3.16) as

$$\varphi_r - \varphi_a = \frac{2\pi}{\lambda_1}(\theta_1 - \theta_r)x_2', \tag{3.18}$$

an expression depending only on the angle subtended at the hologram by the distance separating P and R. If points P and R are at an infinite distance from the hologram ($z_r = z_1 = \infty$, while $x_r/z_r \approx \theta_r$ and $x_1/z_1 \approx \theta_1$ are still finite), Eq. (3.18) continues to hold. The waves arriving at the hologram from point sources at infinity are plane waves. They are the far-field pattern or Fourier transforms of the point sources. Hence the linear fringe system of Eq. (3.18) can be regarded as the interference of a plane wave reference with the Fourier transform of the subject point source P. Not only can the hologram formed as in Fig. 3.4 be illuminated with the original reference point R to produce an image of P, but it can equally well be illuminated by a plane wave to reconstruct a plane wave which is the Fourier transform

of P. In the latter case the reconstructed wave must be observed in the far field to obtain the image of P. The required second Fourier transformation can be performed optically by placing a lens adjacent to the hologram and observing the focal pattern in the back focal plane of the lens. A further discussion of the lensless Fourier transform hologram is given in Chapter 8.

By placing the reference source close to the subject, $x_1 - x_r$ in Eq. (3.17) can be kept small and the fringe frequency ξ' kept low. To the extent that the approximations leading to Eq. (3.3) hold, ξ' is constant across the hologram plate, and holograms can be formed on plates of low resolution. For extended subjects, $x_1 - x_r$ is a function of the width of the subject. Fringes produced by extreme portions of the subject may yet exceed the plate resolution, thus preventing these portions from being recorded. However, for small subjects the lensless Fourier transform hologram configuration produces a uniform, low-frequency fringe system over a large plate area. The result is a wide-aperture hologram which images with high resolution.

Equation (3.18) may be used to express the fringe separation, $d = 1/\xi'$, for the interference pattern formed by the intersection of two plane waves:

$$d = \lambda_1/(\theta_1 - \theta_r). \tag{3.19}$$

Suppose that as in Section 1.3.1, $\theta_r = -\theta_1$. Substituting into Eq. (3.19) we obtain

$$2\theta_1 d = \lambda_1 \tag{3.20}$$

which is a small-angle approximation to Eq. (1.10)

$$2d \sin\theta = \lambda.$$

That the lensless Fourier transform hologram is equivalent to the hologram record of two intersecting plane waves is understandable when one notes that in $(\varphi_r - \varphi_a)$ are phase expressions for two spherical waves of equal but opposite curvature. Phase contributions due to curvature of the wavefronts cancel leaving only those contributions due to the difference in mean directions of the waves.

3.2 Reconstruction with a Point Source

Having considered various hologram-forming arrangements, let us now investigate the reconstruction process. We assume that it is possible to magnify or demagnify the hologram after formation and before reconstruction. To take account of this, the hologram plane coordinates are

relabeled $x_2 = mx_2'$ and $y_2 = my_2'$, where m is the linear magnification. We also assume that the reconstructing wavelength λ_2 need not be the same as the forming wavelength λ_1; their ratio is given by $\mu = \lambda_2/\lambda_1$. The reconstructing or illuminating wave originates from a point source $C(x_c, y_c, z_c)$ as in Fig. 3.5. We do not require C to be the original reference source; it may be the source of a diverging wave or the focus of a converging wave.

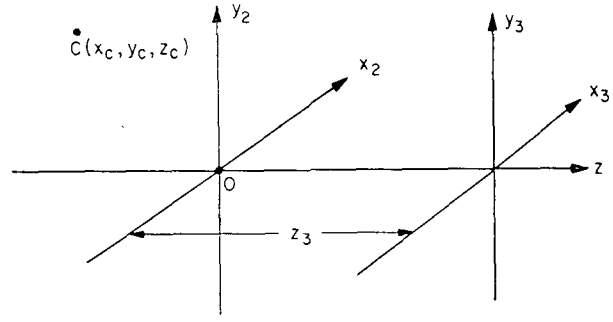

FIG. 3.5. Illumination of a hologram in plane x_2y_2 with a point source $C(x_c, y_c, z_c)$. The image plane can be separated from the hologram by a positive distance z_3, as shown (in which case the image is real), or by a negative distance (virtual image).

When the hologram is properly recorded in photographic emulsion, its amplitude transmittance t is proportional to the intensity I given by Eq. (3.1) (see also Section 1.8), where the spherical wave intensities $I_1 = a_0^2$ and $I_2 = r_0^2$ are approximately uniform over the hologram plane. Hence for holograms of point sources, diffraction results only from illumination of the spatially varying interference terms in the transmittance proportional to

$$\mathbf{ra}^* + \mathbf{r}^*\mathbf{a}.$$

The complex amplitudes of the diffracted waves at the hologram plane are proportional to the products of the illumination complex amplitude $\mathbf{c}$ times the above transmittance terms,

$$\mathbf{cra}^* + \mathbf{cr}^*\mathbf{a},$$

where $\mathbf{c} = c_0 \exp(i\varphi_c)$. In Section 1.8 it is said that the first term above, containing $\mathbf{a}^*$, yields a real image while the second, containing $\mathbf{a}$, produces a virtual image. As we shall see, this is not always the case. Nevertheless the phase of the diffracted wave

$$\mathbf{cra}^* = c_0 r_0 a_0 \exp[i(\varphi_c + \varphi_r - \varphi_a)]$$

is to be labeled

$$\varphi_R = \varphi_c + \varphi_r - \varphi_a, \tag{3.21}$$

while the phase of the wave **cr*a** is to be labeled

$$\varphi_V = \varphi_c - \varphi_r + \varphi_a. \tag{3.22}$$

As in the computation of φ_a, we can cause the phase φ_c of wave **c** to be zero at the origin O and calculate the relative phase at some arbitrary point (x_2, y_2) on the hologram plane. Thus

$$\varphi_c(x_2, y_2) \approx \frac{2\pi}{\lambda_2}\left[\frac{1}{2z_c}(x_2^2 + y_2^2 - 2x_2x_c - 2y_2y_c)\right]. \tag{3.23}$$

The axial distance z_c can be either positive or negative corresponding to illumination by a converging or diverging wave respectively. We can now substitute into Eq. (3.22) the values of φ_c, φ_a, and φ_r, given in Eqs. (3.23), (3.3), and (3.4), respectively, to obtain

$$\begin{aligned}\varphi_V = {} & \left(\frac{2\pi}{\lambda_2}\right)\left(\frac{1}{2}\right)\left(\frac{x_2^2 + y_2^2 - 2x_2x_c - 2y_2y_c}{z_c}\right) \\ & + \frac{2\pi}{\lambda_1}\left(\frac{1}{2}\right)\left(\frac{x_2'^2 + y_2'^2 - 2x_2'x_1 - 2y_2'y_1}{z_1}\right) \\ & - \frac{2\pi}{\lambda_1}\left(\frac{1}{2}\right)\left(\frac{x_2'^2 + y_2'^2 - 2x_2'x_r - 2y_2'y_r}{z_r}\right).\end{aligned}$$

Introducing $x_2 = mx_2'$, $y_2 = my_2'$, and $\mu = \lambda_2/\lambda_1$,

$$\begin{aligned}\varphi_V(x_2, y_2) = {} & \frac{\pi}{\lambda_2}\left[(x_2^2 + y_2^2)\left(\frac{1}{z_c} + \frac{\mu}{m^2z_1} - \frac{\mu}{m^2z_r}\right)\right. \\ & \left. - 2x_2\left(\frac{x_c}{z_c} + \frac{\mu x_1}{mz_1} - \frac{\mu x_r}{mz_r}\right) - 2y_2\left(\frac{y_c}{z_c} + \frac{\mu y_1}{mz_1} - \frac{\mu y_r}{mz_r}\right)\right].\end{aligned} \tag{3.24}$$

Similarly

$$\begin{aligned}\varphi_R(x_2, y_2) = {} & \frac{\pi}{\lambda_2}\left[(x_2^2 + y_2^2)\left(\frac{1}{z_c} - \frac{\mu}{m^2z_1} + \frac{\mu}{m^2z_r}\right)\right. \\ & \left. - 2x_2\left(\frac{x_c}{z_c} - \frac{\mu x_1}{mz_1} + \frac{\mu x_r}{mz_r}\right) - 2y_2\left(\frac{y_c}{z_c} - \frac{\mu y_1}{mz_1} + \frac{\mu y_r}{mz_r}\right)\right].\end{aligned} \tag{3.25}$$

If the hologram is indeed to image the point-source subject P, the phases of the reconstructed waves at the hologram, φ_V and φ_R, must correspond

to those of spherical waves. A first-order approximation to a spherical-wave phase distribution over the hologram can be written, as in Eq. (3.3),

$$\varphi(x_2, y_2) = \frac{2\pi}{\lambda_2}\left[\frac{1}{2z_3}(x_2^2 + y_2^2 - 2x_2x_3 - 2y_2y_3)\right]. \tag{3.26}$$

In the above equation, z_3 is the hologram-to-image plane separation while x_3 and y_3 represent the coordinates of the image point P in the image plane (see Fig. 3.5). We must try to arrange φ_V and φ_R to have the same form as φ. If this can be done, then the image waves are, to first order, spherical and converge or diverge according to the signs of φ_V and φ_R. They represent the case of perfect first-order imaging of the point source. The higher-order terms, neglected in the expansion of φ, φ_V, and φ_R, however, may differ and so represent aberrations (see Section 3.4).

3.3 Characteristics of the Images

By factoring out the coefficient of $(x_2^2 + y_2^2)$ in φ_V and φ_R, one can produce the desired form, indicating perfect first-order imaging. The image coordinates (x_{3V}, y_{3V}, z_{3V}) for φ_V and (x_{3R}, y_{3R}, z_{3R}) for φ_R can be identified as

$$\begin{aligned} z_{3V} &= \left(\frac{1}{z_c} + \frac{\mu}{m^2z_1} - \frac{\mu}{m^2z_r}\right)^{-1} = \frac{m^2z_cz_1z_r}{m^2z_1z_r + \mu z_cz_r - \mu z_cz_1}, \\ x_{3V} &= \frac{m^2x_cz_1z_r + \mu mx_1z_cz_r - \mu mx_rz_cz_1}{m^2z_1z_r + \mu z_cz_r - \mu z_cz_1}, \\ y_{3V} &= \frac{m^2y_cz_1z_r + \mu my_1z_cz_r - \mu my_rz_cz_1}{m^2z_1z_r + \mu z_cz_r - \mu z_cz_1}, \end{aligned} \tag{3.27}$$

and

$$\begin{aligned} z_{3R} &= \left(\frac{1}{z_c} - \frac{\mu}{m^2z_1} + \frac{\mu}{m^2z_r}\right)^{-1} = \frac{m^2z_cz_1z_r}{m^2z_1z_r - \mu z_cz_r + \mu z_cz_1}, \\ x_{3R} &= \frac{m^2x_cz_1z_r - \mu mx_1z_cz_r + \mu mx_rz_cz_1}{m^2z_1z_r - \mu z_cz_r + \mu z_cz_1}, \\ y_{3R} &= \frac{m^2y_cz_1z_r - \mu my_1z_cz_r + \mu my_rz_cz_1}{m^2z_1z_r - \mu z_cz_r + \mu z_cz_1}. \end{aligned} \tag{3.28}$$

Along with the relations defining the image location, we can define expressions for the lateral magnification M_{lat} as

$$M_{lat} \equiv \frac{dx_3}{dx_1} = \frac{dy_3}{dy_1},$$

from which we obtain

$$M_{\text{lat,V}} = m\left(1 + \frac{m^2 z_1}{\mu z_c} - \frac{z_1}{z_r}\right)^{-1},$$
$$M_{\text{lat,R}} = m\left(1 - \frac{m^2 z_1}{\mu z_c} - \frac{z_1}{z_r}\right)^{-1}, \tag{3.29}$$

and the angular magnification M_{ang} as

$$M_{\text{ang}} = \frac{d(x_3/z_3)}{d(x_1/z_1)},$$

from which we obtain

$$|M_{\text{ang}}| = \mu/m. \tag{3.30}$$

3.3.1 In-Line Hologram Images

The letters V and R refer to the reconstructed waves **cr*a** and **cra***, respectively. Whether the images produced by these waves are actually virtual or real depends upon their divergence or convergence, i.e., upon the sign of z_{3V} and z_{3R}. A negative value implies a diverging wave and a virtual image; a positive value implies a converging wave and a real image. (*Note*: z_1, the subject-to-hologram distance, has a negative value if the subject is a real object.) We shall begin our analysis of image characteristics with Gabor's in-line holography where reference, subject, and illuminating sources are all *on axis* so that

$$x_r = x_1 = x_c = 0.$$

Only the x and z components of the image coordinates will be analyzed, since no new information is obtained by considering the y component.

Gabor's "projection method" required that the subject be placed close to the source, i.e., $z_r = z_1 + \Delta$ where Δ is a negative distance and where $\Delta/z_1 \ll 1$ (see Section 2.2). Suppose $\mu = m = 1$ and $z_c = z_r$. (This corresponds to Gabor's all-optical verification of his invention.) With the above x and z values Eqs. (3.27) and (3.28) give

$$x_{3V} = 0, \qquad z_{3V} = z_1 = z_c - \Delta,$$
$$x_{3R} = 0, \qquad z_{3R} = \left(\frac{2}{z_c} - \frac{1}{z_1}\right)^{-1} \approx z_c + \Delta. \tag{3.31}$$

The images lie close to and symmetric about the illuminating source. Since

z_c is negative, *both* images are *virtual*. To photograph these, Gabor needed a lens to form real images at a photographic plate.

For $\mu = m = 1$, the lateral magnification in Eq. (3.29) becomes

$$M_{\text{lat,V}} = \left[1 + z_1\left(\frac{1}{z_c} - \frac{1}{z_r}\right)\right]^{-1},$$
$$M_{\text{lat,R}} = \left[1 - z_1\left(\frac{1}{z_c} + \frac{1}{z_r}\right)\right]^{-1}. \tag{3.32}$$

When the illuminating source is located at the original reference source position $z_c = z_r$, then $M_{\text{lat,V}} = 1$ and $M_{\text{lat,R}} \simeq -1$, remembering that $z_1/z_r \approx 1$. (The -1 magnification in the case of the virtual image produced by φ_R indicates an inverted image.) When the illuminating wavefront has *less curvature* at the hologram than the reference wave, i.e., $|z_c| > |z_r|$, the lateral magnification increases. It becomes large, approaching z_1/Δ as $z_c \to \infty$ and the illumination becomes a plane wave. However the corresponding value of the image plane distance z_3 becomes large as well. The angular magnification, $M_{\text{ang}} = \mu/m = 1$, remains constant.

Gabor's original plan was to form the hologram at electron wavelengths and illuminate it at optical wavelengths. For this case $\mu = \lambda_2/\lambda_1 \simeq 10^5$. To avoid aberrations, he planned to scale the hologram by a factor $\mu = m$ and to place the illuminating source at distance $z_c = mz_r$ from the hologram. The lateral magnification under these conditions becomes

$$M_{\text{lat}} = \pm m = \pm\mu, \tag{3.33}$$

but the angular magnification remains unity. Consequently the distance from hologram to image plane is μ times the distance between object and hologram.

The essential feature of the "*transmission method*" of Haines and Dyson (see Section 2.2) was to place the subject close to the hologram so that $|z_1| \ll |z_r|$. Again with $x_r = x_1 = x_c = 0$, $\mu = m = 1$, and $z_c = z_r$, we obtain from Eqs. (3.27) and (3.28)

$$x_{3V} = 0, \qquad z_{3V} = z_1,$$
$$x_{3R} = 0, \qquad z_{3R} = \left(\frac{2}{z_r} - \frac{1}{z_1}\right)^{-1}. \tag{3.34}$$

If the reference is a plane wave so that $z_r \to \infty$, then a virtual image is found at z_1 and a real image at $-z_1$, the images symmetric this time about the hologram. Both images are upright since in this case $M_{\text{lat,V}} = M_{\text{lat,R}} = +1$.

A result of general consequence, not confined to on-axis holography, can be obtained by considering the hologram to be illuminated by a plane wave ($z_c = \infty$) of wavelength different from that used to form it ($\mu > 1$). With no scaling ($m = 1$), the *lateral magnification* $M_{lat} = (1 - z_1/z_r)^{-1}$ depends on the ratio z_1/z_r but *is independent of the wavelength change*. If, in addition, the reference wave had been a plane wave ($z_r = \infty$), then no magnification whatsoever is obtainable in the reconstruction process. Of course scaling up the dimensions of the hologram can produce large lateral magnification even with plane reference and illuminating waves. However, optical enlargement of the hologram is an impractical and undesirable step in an otherwise lensless imaging process. It also places the image plane at a considerable distance from the hologram. For example, when $z_c = z_r = \infty$ and $\mu = m$, the axial distance of the real image is $z_{3R} = -mz_1 = -\mu z_1$.

3.3.2 Leith–Upatnieks Off-Axis Hologram Images

Leith's and Upatnieks' method allows off-axis positions for the subject, reference, and illuminating sources, and there is no need to restrict the reference source to the z axis as we did in Section 3.1.2. Effects of illuminating the hologram with a wavelength and mean angle different from those of the reference beam can be illustrated easily by assuming plane waves for both reference and illuminating beams. In this section and throughout the remainder of the chapter we shall consider that the hologram dimensions are kept constant so that $m = 1$. Again we confine our attention to the x and z image coordinates. With these simplifications Eqs. (3.27) and (3.28) reduce to

$$x_{3V} = x_1 + \left(\frac{x_c}{z_c}\right)\frac{z_1}{\mu} - \left(\frac{x_r}{z_r}\right)z_1 = x_1 + z_1\left(\frac{\theta_c}{\mu} - \theta_r\right), \qquad z_{3V} = \frac{z_1}{\mu},$$

$$x_{3R} = x_1 - z_1\left(\frac{\theta_c}{\mu} + \theta_r\right), \qquad z_{3R} = -\frac{z_1}{\mu} \tag{3.35}$$

where $\theta_c \approx \tan\theta_c = x_c/z_c$ and $\theta_r \approx \tan\theta_r = x_r/z_r$ are the angles that the illuminating and reference beams make with the positive direction of the z axis (see Fig. 3.6).

When the illuminating wave is identical to the reference, $\mu = 1$ and $\theta_c = \theta_r$. A virtual image then appears at the location of the original subject source (x_1, z_1), and a real image appears in a plane z_1 distant on the other side of the hologram from the illumination sources. Both images are upright.

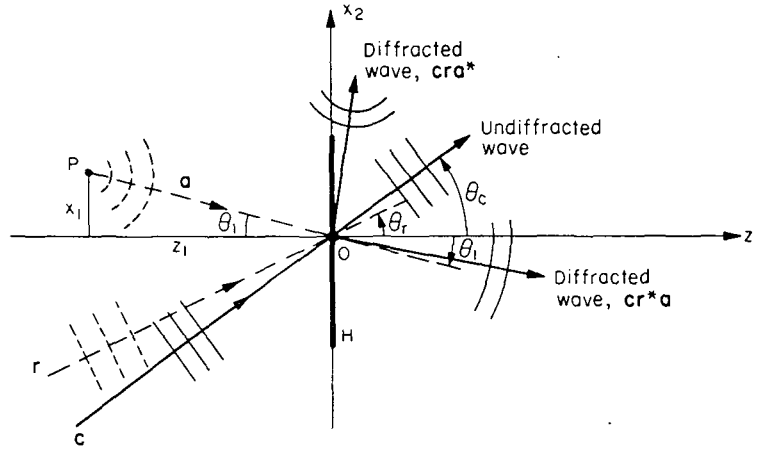

FIG. 3.6. Illumination of Leith–Upatnieks hologram with plane wave **c**. Hologram had been made with spherical wave **a** and plane wave reference **r**. (*Note*: θ_r and θ_c are positive angles while θ_1 is negative.)

As in Section 1.4, it is customary to describe the response of a diffraction grating to incident illumination in terms of the angles of incidence and diffraction. Since holograms discussed in this chapter are similar to plane diffraction gratings, it is appropriate to calculate the diffraction angles corresponding to illumination of a hologram with a plane wave making an angle θ_c to the hologram plane. We can simplify matters further by considering $\theta_c = \theta_r = 0$ as in Fig. 3.7. Then from Eq. (3.35) the diffraction angle corresponding to the φ_V diffracted wave is

$$\theta_{3V} = \frac{x_{3V}}{z_{3V}} = \frac{x_1}{z_1} \approx \theta_1 \qquad \text{(a negative angle for } z_1 < 0\text{)},$$

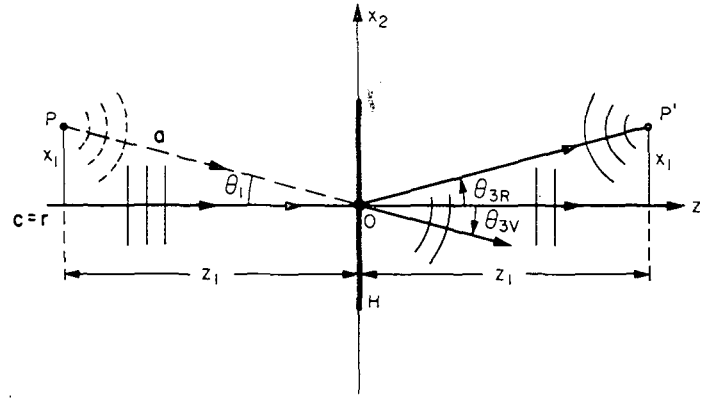

FIG. 3.7. Illumination of off-axis hologram with a plane wave **c** where $\theta_c = \theta_r = 0$.

and the angle corresponding to φ_R is

$$\theta_{3R} = \frac{x_{3R}}{z_{3R}} = -\frac{x_1}{z_1} \approx -\theta_1 \qquad \text{(a positive angle for } z_1 < 0\text{)}.$$

The image waves are as shown in Fig. 3.7. The effect of a wavelength change in the illuminating beam is to multiply the diffraction angles by the wavelength ratio μ. On the other hand for $\mu = 1$ but $\theta_c \neq \theta_r = 0$, the effect is to add θ_c to both θ_{3V} and θ_{3R}, essentially rotating the emerging beams about the y axis.

For the general case of an off-axis reference plane wave and a similar illuminating wave, the diffraction angles obtained from Eq. (3.35) are

$$\theta_{3V} = \mu\theta_1 + \theta_c - \mu\theta_r \quad \text{and} \quad \theta_{3R} = -\mu\theta_1 + \theta_c + \mu\theta_r. \qquad (3.36)$$

A choice of angles often used in making holograms is $\theta_1 = -\alpha$, $\theta_r = +\alpha$ and $\theta_c = +\alpha$. If μ is kept equal to 1, the diffraction angles $\theta_{3V} = -\alpha$ and $\theta_{3R} = +3\alpha$ are as shown in Fig. 3.8.

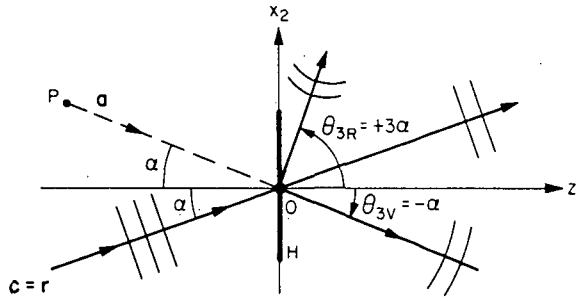

FIG. 3.8. Off-axis hologram made with subject and reference beams symmetric about normal and illuminated with original reference.

Thus far, all of our results have been derived from a first-order approximation. Our analysis, when applied to elementary hologram formation and illumination with plane waves, should yield the familiar plane diffraction grating response, Eq. (1.11)

$$d(\sin i + \sin \delta) = \lambda_2.$$

However the first-order analysis allows only a small angle approximation to Eq. (1.11) to be obtained. To illustrate, let us first restate Eq. (1.11) in a form pertinent to holographically formed gratings. Consider a grating to have been formed by interference of two plane waves on a photographic emulsion as in Fig. 1.4. For the case shown there, each forming angle can

be set equal to θ_1 so that $d = \lambda_1/(2 \sin \theta_1)$. Substituting d into Eq. (1.11) and assuming that an illuminating plane wave is incident at an angle $i = \theta_1$, we obtain for the angle of diffraction δ (which is also the angle θ_3 in the notation of this chapter)

$$\begin{aligned} \sin \delta \equiv \sin \theta_3 &= 2(\lambda_2/\lambda_1) \sin \theta_1 - \sin \theta_1 \\ &= \sin \theta_1(2\mu - 1). \end{aligned} \qquad (3.37)$$

Now let us evaluate the diffraction angle θ_{3V}, in Eq. (3.36), under similar conditions. The conditions are met by setting $\theta_1 = -\theta_r$ and $\theta_c = \theta_r$. We obtain

$$\theta_{3V} = \theta_1(2\mu - 1), \qquad (3.38)$$

the first-order approximation to Eq. (3.37). Thus, results obtained through first-order geometric considerations hold only so long as $\sin \theta \approx \tan \theta \approx \theta$.

3.3.3 Images When All Sources Are Equidistant from the Hologram

Suppose the subject and reference point sources lie in the same plane so that $z_1 = z_r$, and suppose that the illuminating wave is identical to the reference ($x_c = x_r$, $z_c = z_r$). Equations (3.27) and (3.28) reduce to

$$\begin{aligned} x_{3V} &= x_r(1 - \mu) + \mu x_1, \qquad z_{3V} = z_1, \\ x_{3R} &= x_r(1 + \mu) - \mu x_1, \qquad z_{3R} = z_1. \end{aligned} \qquad (3.39)$$

The configuration forms the lensless Fourier transform hologram, and in this case both images are virtual, lying in the original subject plane. If the reference source lies on the z axis, then the images are symmetric about the z axis. The image at (x_{3R}, z_{3R}) is inverted.

Any of the waves can be converging to a point which is a positive distance from the hologram plane. Suppose the subject beam is such a converging beam so that z_1 is positive and suppose $z_r = z_c = -z_1$. Then

$$z_{3V} = z_1/(2\mu - 1),$$

and the image produced by φ_V is real, for $2\mu > 1$. On the other hand the image produced by φ_R is characterized by

$$z_{3R} = -z_1/(2\mu + 1)$$

and is virtual. If, instead, it is the illuminating wave that is chosen to be converging to a point a positive distance from the hologram, then inspection of z_{3V} and z_{3R} in Eqs. (3.27) and (3.28) reveals that both images are real; in this case the image at (x_{3V}, z_{3V}) is inverted.

3.4 Third-Order Aberrations

Equation (3.26) representing a spherical-wave phase distribution over the hologram is only a first-order approximation in $1/z_3$. The next order of approximation consists of a number of terms all multiplying the factor $(1/z_3)^3$. This is also true, of course, of the expressions for φ_a, φ_r, and φ_c in Eqs. (3.3), (3.4), and (3.23), respectively. The third-order terms of Eqs. (3.3), (3.4), and (3.23) are to be added together in accordance with Eq. (3.21) or (3.22) to give the third-order terms in φ_V or φ_R. The phase differences between the third-order expansion of Eq. (3.26) and the third-order expansion of φ_V (or φ_R) are the aberrations.

Meier [*3.2*] has calculated hologram aberrations in terms of their usual classifications: spherical aberration, coma, astigmatism, field curvature, and distortion. He finds that one or the other of the waves diffracted by the hologram yields an image free of all aberrations providing the illuminating wave is identical with the reference. For this case the magnification is unity. Magnification is achieved (1) by illuminating the hologram with a spherical wave whose curvature differs from the reference, keeping $\mu = m = 1$; (2) by illuminating with a wavelength differing from that used to form the hologram, $\mu \neq 1$; and (3) by scaling the hologram, $m \neq 1$. The first method cannot be employed without producing aberrations. If plane waves are used for reference and illumination, then the condition $\mu = m$ and $\theta_c = \theta_r$ produces an aberration-free image from φ_V, while $\mu = m$, $\theta_c = -\theta_r$ produces an aberration-free image from φ_R. (The scaling, however, requires a lens which may degrade the image.) When reference source and subject sources are equidistant from the hologram (the lensless Fourier transform configuration, $z_1 = z_r$), magnification can be achieved without optical scaling and with zero spherical aberration. The magnification is obtained by making $\mu > 1$. However at least one of the other aberrations will be present.

REFERENCES

3.1. J. C. Urbach and R. W. Meier, "Thermoplastic Xerographic Holography," *Appl. Opt.* **5**, 666 (1966).

3.2. R. W. Meier, "Magnification and Third-Order Aberrations in Holography," *J. Opt. Soc. Amer.* **55**, 987 (1965).

3.3. E. B. Champagne, "Nonparaxial Imaging, Magnification, and Aberration Properties in Holography," *J. Opt. Soc. Amer.* **57**, 51 (1967).

3.4. J. T. Winthrop and C. R. Worthington, "X-Ray Microscopy by Successive Fourier Transformation," *Phys. Lett.* **15**, 124 (1965).

3.5. G. W. Stroke, "Lensless Fourier-Transform Method for Optical Holography," *Appl. Phys. Lett.* **6**, 201 (1965).

Chapter 4

THE FOURIER TRANSFORM

The analysis of point-source holograms, presented in Chapter 3, is based on the determination of differences in geometrical path to the hologram taken by simple spherical or plane waves issuing from point sources. For such simple waves, the complex light amplitude in the immediate vicinity of the hologram can be easily specified; fundamental aspects of hologram formation and wavefront reconstruction are then describable in terms of this complex amplitude. When, on the other hand, a complicated distribution of light complex amplitude exists in an input plane, and it is desired to know how this distribution is modified by passage through free space, optical components, holograms, and other obstacles, then consideration must be given to more general light wave propagation.

Electromagnetic waves can be temporally modulated or, as is generally the case at optical wavelengths, they can be spatially modulated. When temporally modulated, the wave propagation may be analyzed in either of two domains: a temporal domain or a temporal-frequency domain. Analogously, spatially modulated wave propagation, which is our concern here, may be analyzed in either a spatial domain or a spatial-frequency domain. In the spatial domain the light complex amplitude $\mathbf{a}(x, y)$ is expressed as a function of the x, y spatial coordinates of an observation plane through which the light propagates. The same complex amplitude distribution can be expressed in terms of orthogonal spatial frequencies ξ and η as well. According to the basic theorem of Fourier analysis, as applied to light distributions, any two-dimensional complex amplitude pattern can be considered as a discrete or continuous set of sinusoidally varying patterns (periodic components). The reciprocal of the spatial period of any of the